RSC Advances

PAPER

View Article Online
View Journal | View Issue

Cite this: *RSC Adv.*, 2020, **10**, 42363

Influence of the heteroatom introduction on the physicochemical properties of 5-heterotruxenes containing nitrogen, oxygen and sulfur atom†

Krzysztof Górski, * Krzysztof Noworyta and Justyna Mech-Piskorz

Received 31st August 2020
Accepted 15th November 2020

DOI: 10.1039/d0ra07483g

rsc.li/rsc-advances

5-heterotruxenes are a class of heterocyclic aromatic compounds derived from the parent heptacyclic hydrocarbon, namely truxene. Currently, few substances belonging to this group are known. These include derivatives of 5-oxatruxene, 5-azatruxene, and 5-thiatruxene, along with its sulfone and sulfoxide. The introduction of one heteroatom, not only enables selective monofunctionalization of the 5-heterotruxene system but also allows adjustment of physico-chemical properties depending on the needs. Two investigated compounds, namely 5-oxatruxene and 5-azatruxene, exhibit fluorescence enhancement by symmetry breaking (FESB) phenomena, manifested by a fourfold increase in the fluorescence quantum yield. Therefore, derivatives of 5-heterotruxenes may contribute to the development of new stable optoelectronic substances as well as other functional materials. Nevertheless, in the beginning, it is crucial to investigate their spectral, thermal, and electrochemical properties to learn more about the advantages and limitations of these aromatic systems. The following article also presents a new simplified and universal synthetic methodology, without use of anhydrous conditions or organometallic substances, giving easy access to 5-azatruxene and structural-related heteroaromatic systems. The discussed heteroatom influence is not limited to the truxene core but also helps to understand the physicochemical properties of other, currently top-rated high-symmetric heteroaromatic systems such as circulenes, sumanenes and their analogues.

Introduction

Truxenes, as functional materials, have a long and rich history. Initially, these materials aroused interest in the dynamically developing LCD industry. Various polymorphic structures, and the excellent thermal and chemical stabilities of alkyl derivatives of truxenes make them desired candidates for LCDs.[1–3] Further studies of this group of compounds enabled the development of "self-healing" displays.[4] Exploration of truxene alkyl derivatives towards non-linear optical properties,[5] including three-photon absorption[6] is on-top. Emissive properties of truxene derivatives makes them useful also as lasing materials[7–9] or as fluoride ion sensors.[10] The development of optoelectronic, in particular OLED and OPV technologies, has boosted interest in the truxene.[11] Moreover truxenes are scaffolds of efficient polymerization photocatalyst, activated by visible light, applicable in 3D printing.[12–16] The insertion of the heteroatom into the truxene scaffold is a relatively simple modification of the extended π-electronic structure, Fig. 1. The most studied heterotruxenes are the systems with three heteroatoms of one type introduced into three five-membered rings. Synthesis of this symmetrical 5,10,15-triheterotruxenes is relatively simple and enables adjustment of individual properties.[17–19] It was proven that both trithiatruxene[20–22] and triazatruxene[23–26] derivatives exhibit good hole conductivity, which is crucial in the prototype photovoltaic devices. Attachment of an acceptor unit to the truxene or 5,10,15-triazatruxene

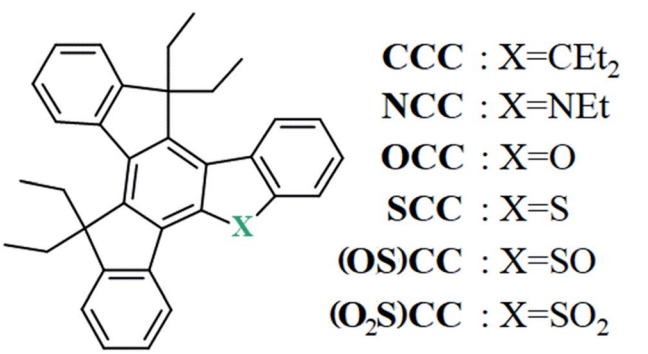

Fig. 1 Structure of ethylated 5-heterotruxenes.

Institute of Physical Chemistry, Polish Academy of Sciences, Kasprzaka 44/52, 01-224 Warsaw, Poland. E-mail: kgorski@icho.edu.pl

† Electronic supplementary information (ESI) available: Synthesis protocol for **NCC** and bromoderivatives of **OCC** and **NCC**, cyclic voltammograms for **CCC**, **NCC**, **OCC**, **SCC**, **(OS)CC** and **(O2S)CC**, spectral radiation distribution of UV-C lamp, NMR spectra. See DOI: 10.1039/d0ra07483g

results in ambipolar semiconductors,[27–31] or light-harvesting materials[32–36] used in Dye Sensitized Solar Cells (DSSC). In addition, many truxene[37,38] and 5,10,15-triazatruxene[39–43] derivatives are tested towards OLEDs blue emitters. Appropriate design of truxene and 5,10,15-triazatruxene based materials also allows the detection of vapours of explosive substances,[44–48] hydrazine,[49] or hydrogen chloride.[50] It was found that 5,10,15-triazatruxene derivatives can detect even biologically active substances.[51,52] In the donor–acceptor system, the use of an unsymmetrical derivative of heterotruxene, namely 5-thiatruxene, as an acceptor, resulted in a very stable third-generation deep-blue emitters fulfilling requirements for HD OLED displays.[53,54] This type of emitters utilize thermally activated delayed fluorescence (TADF), where proper location of energy levels (singlet and triplet states) within the heterotruxene is responsible for reduced TADF lifetime.[55] Excellent thermal and chemical stability together with relatively easy modulation of optical and electrical properties drives further research of heterotruxenes towards new unsymmetrical structures. This paper describes the new, simplified and allowing the introduction of most p-block heteroatoms synthesis of 5-heterotruxenes. Moreover, properties of five soluble heterotruxenes, namely 5-oxatruxene, 5-azatruxene, and 5-thiatruxene (3 forms with various oxidation states) are studied in detail. The synthesized compounds show improved fluorescence yields, and thermal stability, compering truxene **CCC**, as well as tendency to form stable amorphous phases. Their properties make them interesting materials for optoelectronic applications.

Results and discussion

Synthetic procedures

Compound **CCC** was synthesized according to known literature procedures,[56] and **OCC**, **SCC**, **(OS)CC**, and **(O2S)CC** were obtained using synthetic routes published by our group.[57,58] Herein we describe an alternative synthetic pathway, improving on the initial approach, to access azatruxene derivative **NCC**, which we very recently reported for the first time.[58] 2-(Indan-1-ylidene)indan-1-one **1**, which is a product of the acid promoted, silicon mediated aldol cross-condensation of indan-1-one, turned out to be a valuable building block in the synthesis of **OCC** and **SCC**. Moreover, **1** is a promising precursor for the synthesis of other 5-heterotruxenes, containing different p-block heteroatom The acid promoted aldol cross-condensation between α,β-unsaturated ketone **1** and acetophenone **2** leads to the phenyl derivative of 7,12-dihydroindeno[1,2-*a*]fluorene **5**, Scheme 1. Condensation in the presence of methanesulfonic acid, at room temperature, after 14 days leads to **5** with the reaction yield of 48%. Increasing temperature to 90 °C allows a 7-fold reduction of the condensation time, and an increase of the reaction yield to 56%. The increase in the reaction yield is not spectacular due to a side reaction, which is cyclotrimerization of acetophenone **2**, occurring in a strong acid medium.[59–62] In order to minimize the side reaction effect and to increase the contribution of cross-condensation, tetraethoxysilane was added to the reaction mixture. Tetraethoxysilane reduces the activation energy in the condensation process[58] leading to **5** with the reaction yield about 60% in the reduced temperature conditions, 50 °C.

The compound **5**, Scheme 2, after alkylation, is converted to tetraethyl derivative **6**, followed by the nitration in the presence of concentrated nitric(v) acid leading to **7**. An essential step for producing **NCC** is nitrene insertion into the C–H bond. Cadogan's reaction conditions, known from the literature,[63,64] fail in this case. Only the use of solvent-free conditions and an increase of the reaction temperature to 270 °C leads to 10,10,15,15-tetraethyl-5-azatruxene, **8**. Obtained compound, in the presence of ethyl bromide and potassium hydroxide, is finally converted to **NCC**. Overall **NCC** reaction yield is ~60%, which is about two times higher than previously reported

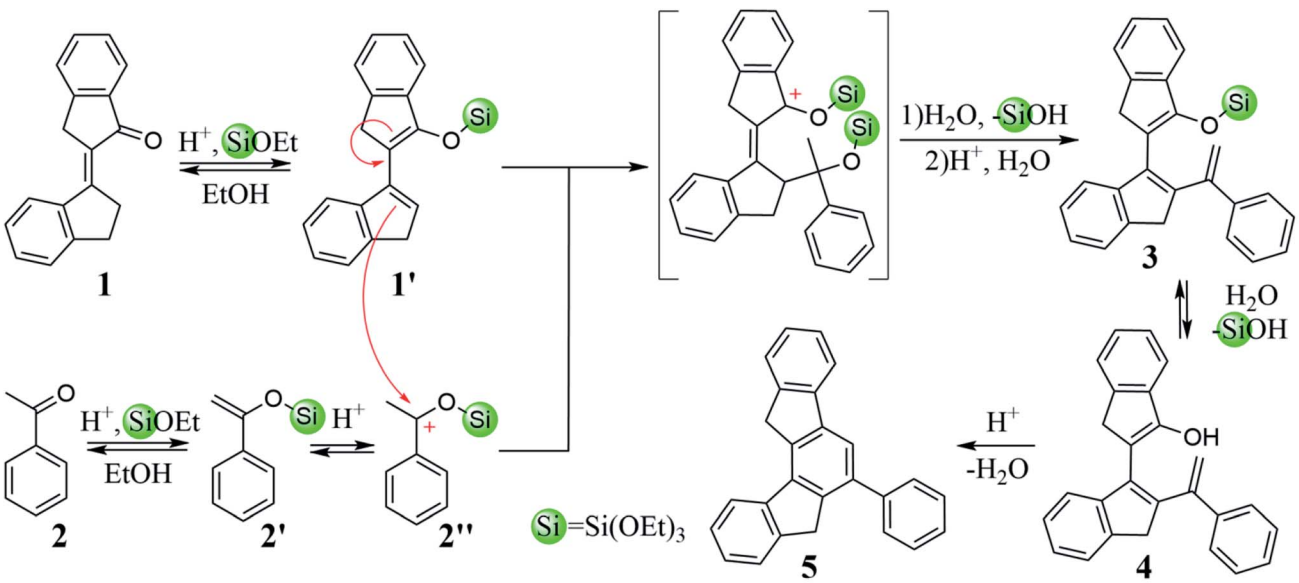

Scheme 1 Proposed mechanism of acid promoted, silicon mediated aldol cross-condensation.

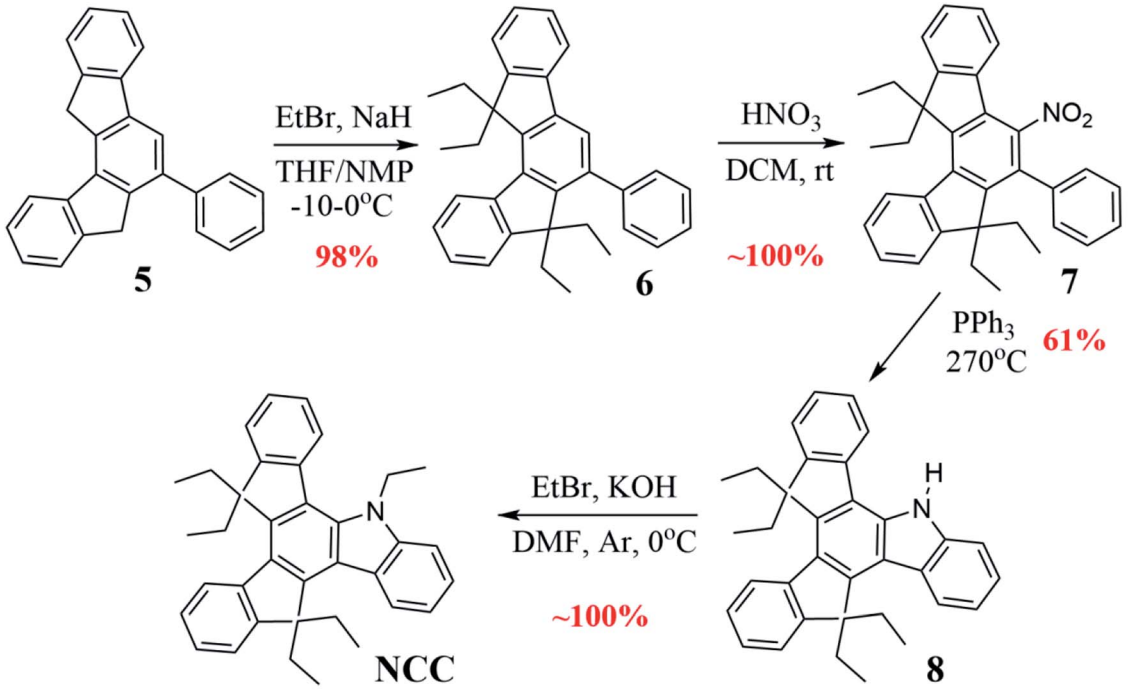

Scheme 2 Synthetic pathway leading to NCC.

method.[58] The presented synthetic approach is an alternative to photocyclization, which allows the efficient synthesis of soluble derivatives of 5-heterotruxenes[57,58] and 5,10-diheterotruxenes.[65] The further development of this methodology may lead to new synthetic approaches of 5-heterotruxenes, as well as to explore the chemistry of unknown class of aromatic systems, namely 7,12-dihydroindeno[1,2-*a*]fluorenes. The reactivity of 5-aza and 5-oxatruxene towards formation of polybrominated derivatives was also examined. For this purpose, **NCC** and **OCC** were reacted with 3.1 eq. of bromine, which resulted in obtaining tribromo derivatives, **9** with reaction yield of 87% and 93% respectively, Scheme 3. It is worth mentioning that in the case of **NCC**, the use 4.1 eq. of bromine leads to a tetrabrominated derivative, **10** with reaction yield of 91%. On the other hand **(OS)CC** and **(O_2S)CC** do not react under this conditions. A detailed description of the synthesis protocol and the bromination procedures of **OCC** and **NCC** are attached to the ESI file.†

The main feature that distinguishes 5-heterotruxenes from truxene is the symmetry of the molecule. The introduction of one heteroatom into the truxene π-electron system results in breaking the C_{3h} symmetry of **CCC**.

Quantum chemical calculations

Quantum chemical calculations have been performed in order to elucidate influence of heteroatom on the electronic properties of the synthesized truxenes. The energy of the HOMO level of 5-heterotruxene, relative to **CCC**, varies from molecule to

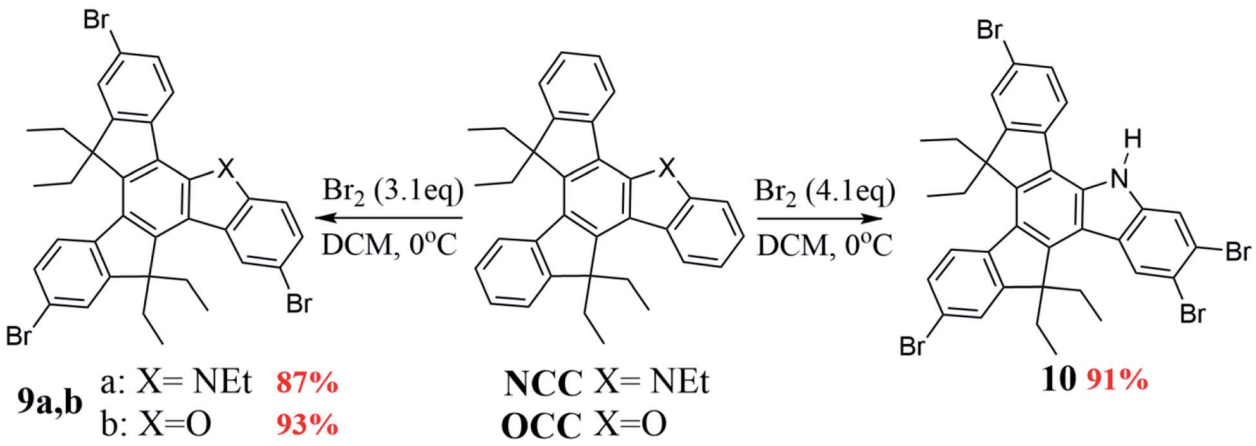

Scheme 3 Bromination of NCC and OCC.

molecule (Fig. 2). However, among heteroaromatic systems with a non-oxidized heteroatom, **NCC**, **OCC**, **SCC**, the observed primary trend is the increase of the HOMO comparing to **CCC**. The highest energy of the HOMO level among investigated 5-heterotruxenes belongs to **NCC** (0.53 eV higher than of **CCC**) as a result of electron-donating properties of a nitrogen atom. The destabilization of the HOMO level in **OCC** is lower than in **NCC**. The lower energy of the HOMO level of **OCC**, comparing to **NCC**, is a result of two competing effects: free electron pairs located on oxygen atom interact with truxene π-electron system, causing the HOMO level to increase, and on the other hand, the high electronegativity of oxygen atom causes stabilization of the HOMO. The resultant destabilization of the HOMO level in **OCC** comparing to **CCC** is 0.16 eV. Replacing an oxygen atom with a sulfur atom decreases the HOMO's stabilization because of the lower electronegativity of the last. As a result, the HOMO of **SCC** is 0.23 eV higher than of **CCC**. Truxenes with oxidized heteroatom *i.e.*, sulfoxide **(OS)CC** and sulfone **(O_2S)CC**, behave differently. The HOMO level of **(OS)CC** and **(O_2S)CC** is respectively 0.21 eV and 0.39 eV below the HOMO of **CCC**.

LUMO levels of almost all considered 5-heterotruxenes are stabilized compared to the LUMO of **CCC** (only **NCC** has the same energy of LUMO than **CCC**). Analogously to the HOMO, it can be explained by few phenomena *i.e.*, electron donation, inductive effect, and orbital degeneracy lifting. While the electron donation destabilizes the LUMO level, the last two phenomena are responsible for its stabilization. From all examined heteroatoms, nitrogen is the most electron-donating, but even in that case, stabilizing effects prevail. Therefore LUMO level of **NCC** has the same value as LUMO of **CCC**. In the case of **OCC** and **SCC**, the electron-donating properties of the introduced atoms are incomparably smaller than in the case of a nitrogen atom. Thus the LUMO stabilization is more visible for **OCC** and **SCC**, with the values 0.13 and 0.15 eV below **CCC** LUMO. The LUMO levels of **(OS)CC** and **(O_2S)CC** are respectively 0.64 eV and 0.85 eV lower than **CCC**. Such meaningful stabilization of the LUMO level primarily results from introduction of electron withdrawing groups such as **SO** and **SO_2**. In addition, **(OS)CC** and **(O_2S)CC** reveals π*–σ* conjugation.[66–68] The phenomenon described for the first time in heteroles of the third period is responsible for significant stabilization of the lowest unoccupied molecular orbital, Fig. 3. The effect mentioned above originates from the overlap between π* orbital, located within the five-membered heterocyclic ring with the σ* orbital of O–S exocyclic bond.

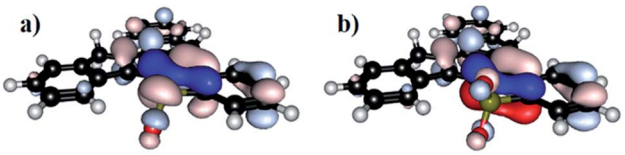

Fig. 3 π*–σ* conjugation observed in the LUMO orbital of (a) **(OS)CC** and (b) **(O_2S)CC**.

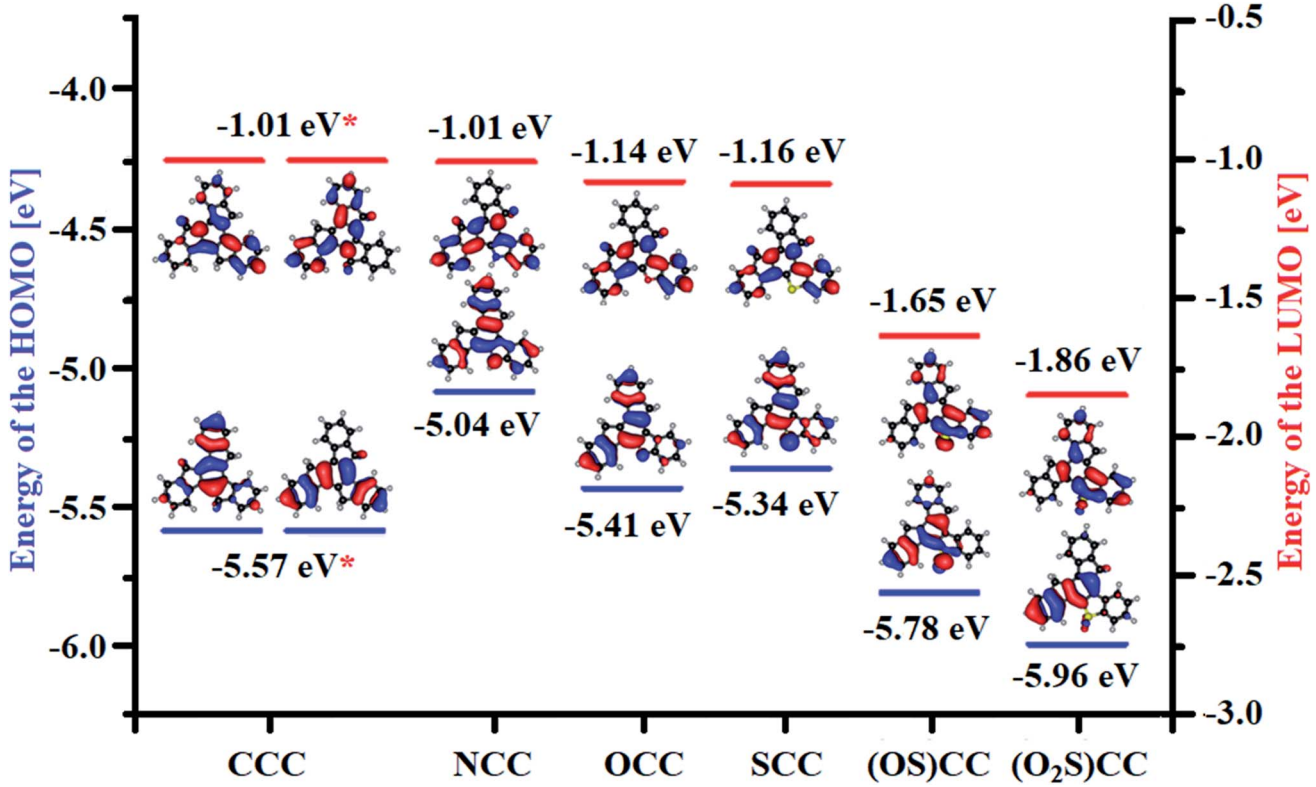

Fig. 2 Theoretical energy diagram of ethylated 5-heterotruxenes. * – double degenerated level.

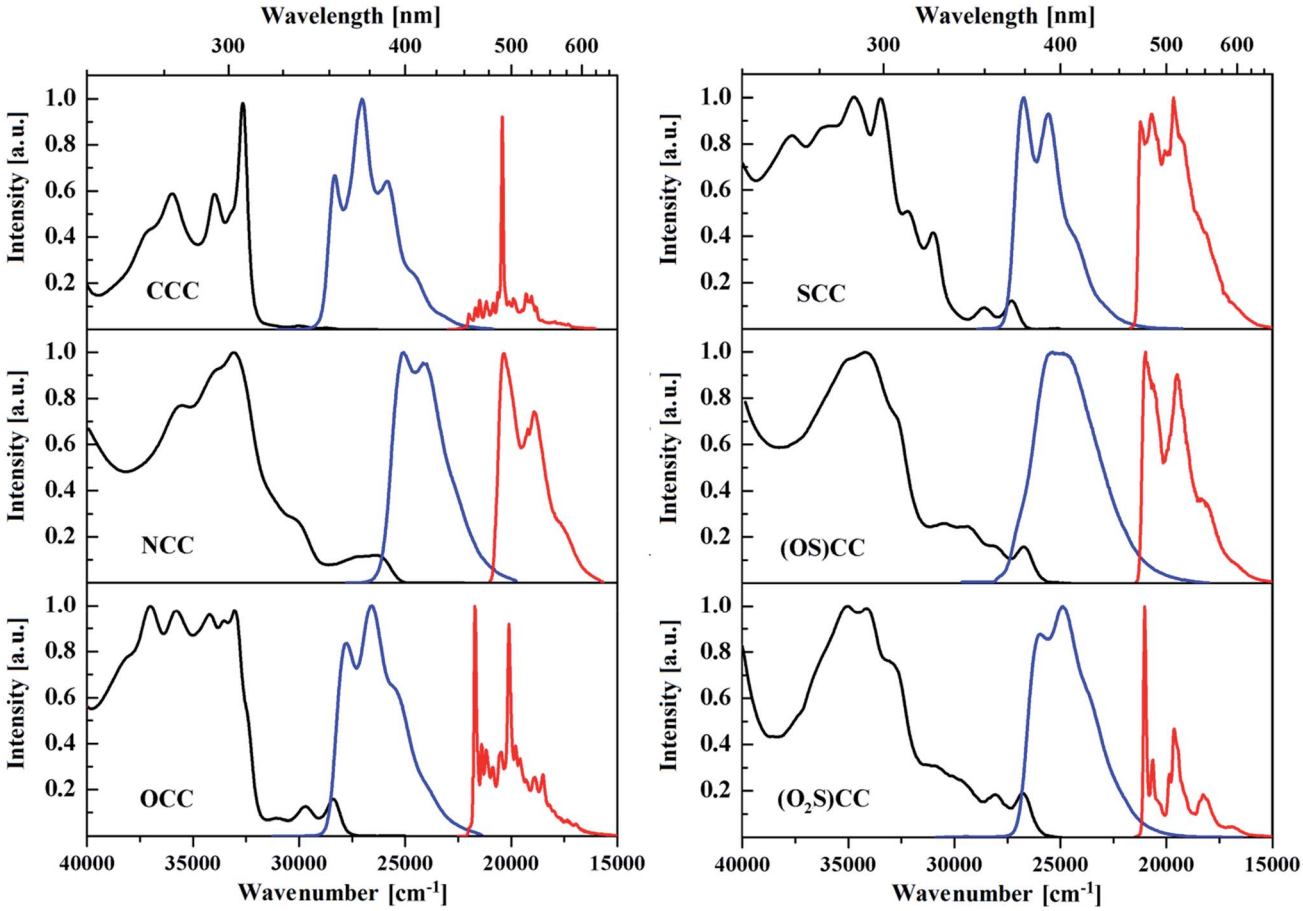

Fig. 4 Normalized absorption (black), fluorescence (blue), and phosphorescence (red) spectra of ethylated 5-heterotruxenes in the solution. Absorption and fluorescence were measured at room temperature in dichloromethane, and phosphorescence was measured at 77 K in methylcyclohexane.

Calculated energies of the molecular orbitals reveal the lowering of the energy gap ($\Delta E_{HOMO-LUMO}$) following the introduction of the heteroatom.

Photophysical properties

Results of spectroscopic studies of the 5-heterotruxenes dissolved in DCM are presented in Fig. 4 and in Table 1. **NCC** reveals the lowest energy of the 0–0 transition ($E_{0-0} = 3.18$ eV) and the largest bathochromic shift, in absorption and emission spectra, compared to **CCC**. **OCC** has the largest 0–0 transition among considered 5-heterotruxenes, $E_{0-0} = 3.48$ eV, followed by **SCC** with $E_{0-0} = 3.35$ eV. The oxidation of 5-thiatruxene to **(OS)CC** and **(O_2S)CC** causes a decrease of energy of the 0–0 transition and a slight red-shift of the absorption and fluorescence

Table 1 Spectroscopic data of ethylated truxene and 5-heterotruxenes in the solution[a,b]

Compound	λ_{abs} [nm]	λ_{flu} [nm]	E_{0-0} [eV]	Φ_{flu} [%]	τ_F [ns]	k_R^S	k_{NR}^S	λ_{phos} [nm]	$T_1 \leftarrow S_0$ [eV]	Φ_{phos}/Φ_{flu}
CCC	294, 306, 333, 348	353, 370, 387	3.54	8.5	18	4.72×10^6	5.08×10^7	454, 490	2.73	0.36
NCC	295, 302, 331, 380	399, 417	3.18	34.8	4	8.70×10^7	1.63×10^8	492, 529	2.52	0.32
OCC	292, 303, 337, 352	360, 377, 393	3.48	36.6	6	6.10×10^7	1.06×10^8	460, 497	2.70	0.08
SCC	311, 323, 350, 367	374, 391	3.35	5.4	2	2.70×10^7	4.73×10^8	472, 483, 509	2.63	3.76
(OS)CC	329, 341, 355, 375	395, 404	3.22	0.8	1	8.00×10^6	9.92×10^8	477, 514, 551	2.60	2.03
(O_2S)CC	324, 337, 357, 373	385, 402	3.27	13.5	2	6.75×10^7	4.33×10^8	476, 485, 509, 548	2.60	0.61

[a] Absorption and fluorescence measured at r.t. in dichlomethane, phosphorescene measured at 77 K in methylcycloexane. [b] λ_{abs}, λ_{flu}, λ_{phos} – wavelengths of the main bands of absorption, fluorescence and phosphorescence spectra respectively, E_{0-0} – the energy of the 0–0 transition, determined from the intersection of absorption and fluorescence spectra, Φ_{flu} – fluorescence quantum yield, τ_F ,-fluorescence lifetime, k_R^S – singlet radiative constant, k_{NR}^S – singlet nonradiative constant, $T_1 \leftarrow S_0$ – the energy difference between T_1 and S_0 estimated from the phosphorescence band of the highest energy, Φ_{phos}/Φ_{flu} – a ratio of phosphorescence and fluorescence quantum yields in the temperature of 77 K.

spectra, compared to **SCC**. A similar red-shift is practically not observed in the series of 5-thiatruxene, in the case of phosphorescence. However, changes in the vibronic structure become even more pronounced. The largest "pseudo-Stokes shift", valued at 4400 cm^{-1} presents **CCC**, due to symmetry forbidden electronic transitions. For the first two transitions (S_0–S_1 and S_0–S_2), the oscillator strength equals 0. However, experimentally the first two transitions are visible, with very low intensities. Such a phenomenon can be explained by coupling between electronic and vibrational states, thereupon transitions S_0–S_1 and S_0–S_2 becomes visible. The direct consequence of introducing one heteroatom into the truxene core is lowering the symmetry of the molecule from C_{3h} to C_s or C_1, making transitions S_0–S_1 and S_0–S_2 allowed. This phenomenon results in the appearance of new low energetic bands in the 5-heterotruxenes absorption spectrum. The described phenomenon leads to fluorescence enhancement by symmetry breaking (FESB),[69] which is manifested by a more than four-fold increase in fluorescence quantum yield of **NCC** and **OCC** compared to **CCC**. On the other hand, the presence of a sulfur atom in the **SCC** lowers its emissive properties. Comparison of low-temperature emission spectra, *i.e.*, fluorescence and phosphorescence of studied 5-heterotruxenes (Fig. 4, Table 1), may indicate an increase of the population of excited triplet state T_1 of **SCC** ($\Phi_{phos}/\Phi_{flu} = 3.76$). The described effect corresponds to the presence of a sulfur atom in a truxene core, which causes a significant increase in the spin–orbit coupling compared to the oxygen atom.[70–72] The increase in the interaction between spin and orbital magnetic moment enhances the intersystem crossing and thus the triplet population. However, about a 7-fold decrease of **(OS)CC** fluorescence quantum yield (Φ_{flu} = 0.8%), compared to **SCC**, cannot be explained solely by the presumed increase of the triplet state population (Φ_{phos}/Φ_{flu} = 2.03). TD DFT calculations made for **(OS)CC** primarily indicate a relatively low oscillator strength for S_0–S_1 transition of about 0.038. Further analysis of the first electronic transition components indicates the participation of three separate processes, of which two of them turn out to be transitions of the n–π* nature. The n–π* transition relies on the transfer of electrons from free pairs located within the SO moiety to the π-electron system of the molecule. Clean n–π* transitions are known for their forbidden nature[73] resulting from the orthogonality of wave functions of the electronic states involved in the excitation process. The presence of n–π* transitions in the **(SO)CC** are responsible for a significant reduction of the emissive properties of the molecule. Further oxidation introduces a second oxygen atom and restores the symmetry plane in the **(O_2S)CC**. Free electron pair located on the sulfur atom now participates in bond

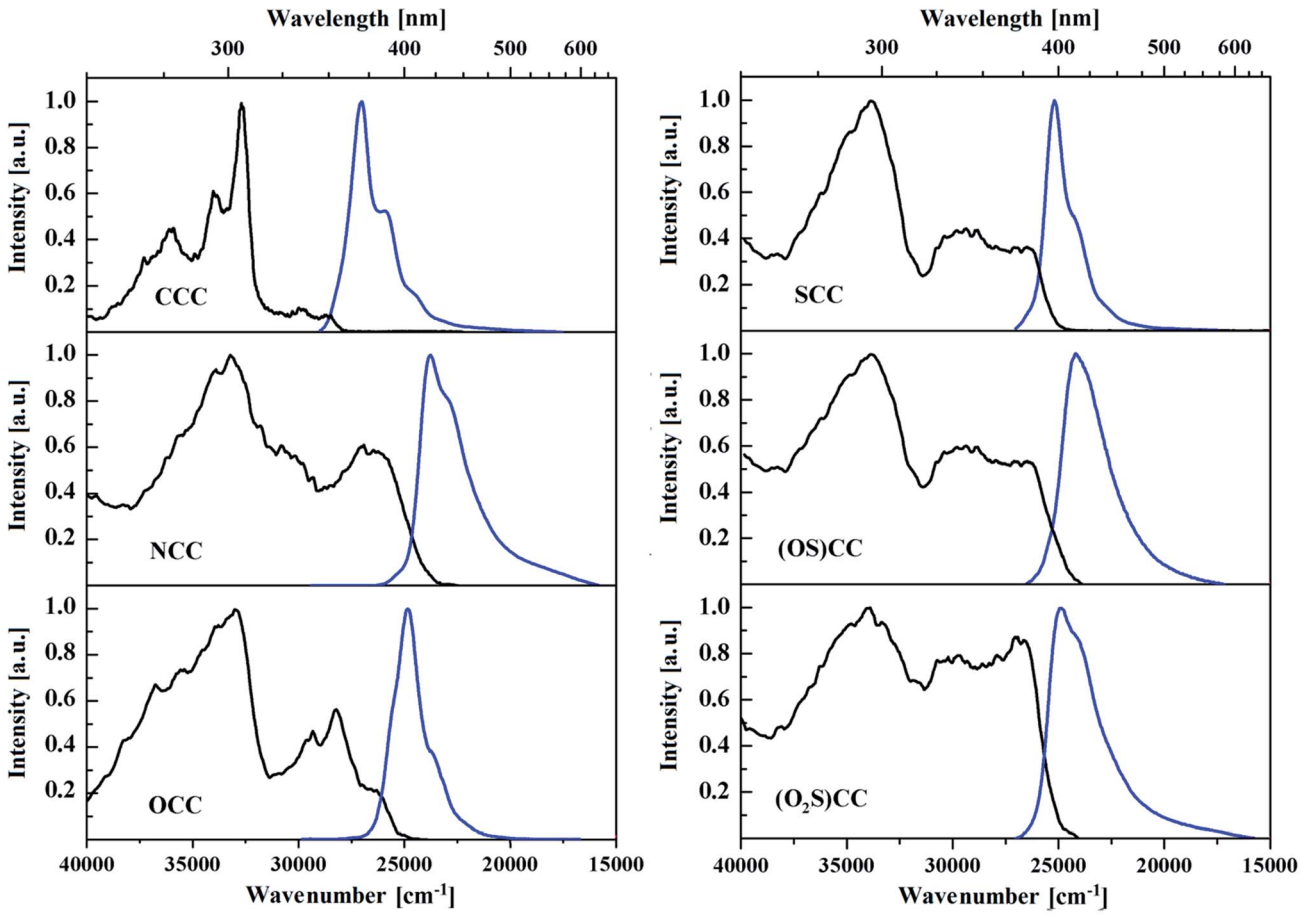

Fig. 5 Normalized absorption (black) and fluorescence (blue) spectra of ethylated 5-heterotruxenes in the solid in powder form.

Table 2 Spectroscopic data of ethylated truxene and 5-heterotruxenes in the solid in powder form[a]

Compound	λ_{abs} [nm]	λ_{flu} [nm]	ΔE [eV]	Φ_{flu} [%]	τ_F [ns]	k_R^S	k_{NR}^S	$\nu(F_{sol}–F_{solid})$ [cm^{-1}]
CCC	294, 306, 335, 349	370, 386	3.35	19.0	34 700	5.48×10^6	2.33×10^7	1301
NCC	301, 325, 372, 381	421	2.95	10.3	2699	5.14×10^7	4.47×10^8	1309
OCC	303, 341, 355, 379	403, 420	3.08	22.0	1700	1.29×10^8	4.59×10^8	2963
SCC	295, 340, 378	397	3.12	3.5	0.848	4.13×10^7	1.14×10^9	1549
(OS)CC	295, 341, 379	413	3.00	0.3	0.333	9.02×10^6	3.00×10^9	1103
(O_2S)CC	294, 338, 376	402	3.08	5.4	0.885	6.10×10^7	1.07×10^9	1098

[a] ΔE – band gap determined from the emission band of the highest energy, λ_{abs}, λ_{flu} – wavelength of absorption and fluorescence, Φ_{flu} – fluorescence quantum yield, $\nu(F_{sol}–F_{solid})$ – red-shift between the fluorescence spectrum in the solution and the fluorescence spectrum in the solid in powder form.

formation with the oxygen atom, causing that the three processes involved in the transition S_0–S_1 becomes π–π^* type. The result is more than a 2-fold increase in oscillator strength for the first electron transition to 0.087. The introduction of the second oxygen atom reduces Φ_{phos}/Φ_{flu} rate to 0.61 and probably the triplet state population. The synergy of both effects causes a 17-fold increase of **(O_2S)CC** fluorescence quantum yield in solution up to 13.5%, corresponding to **(OS)CC**.

By passing from a solution to a solid state, the spectroscopic properties of 5-heterotruxenes are noticeably different (Fig. 5

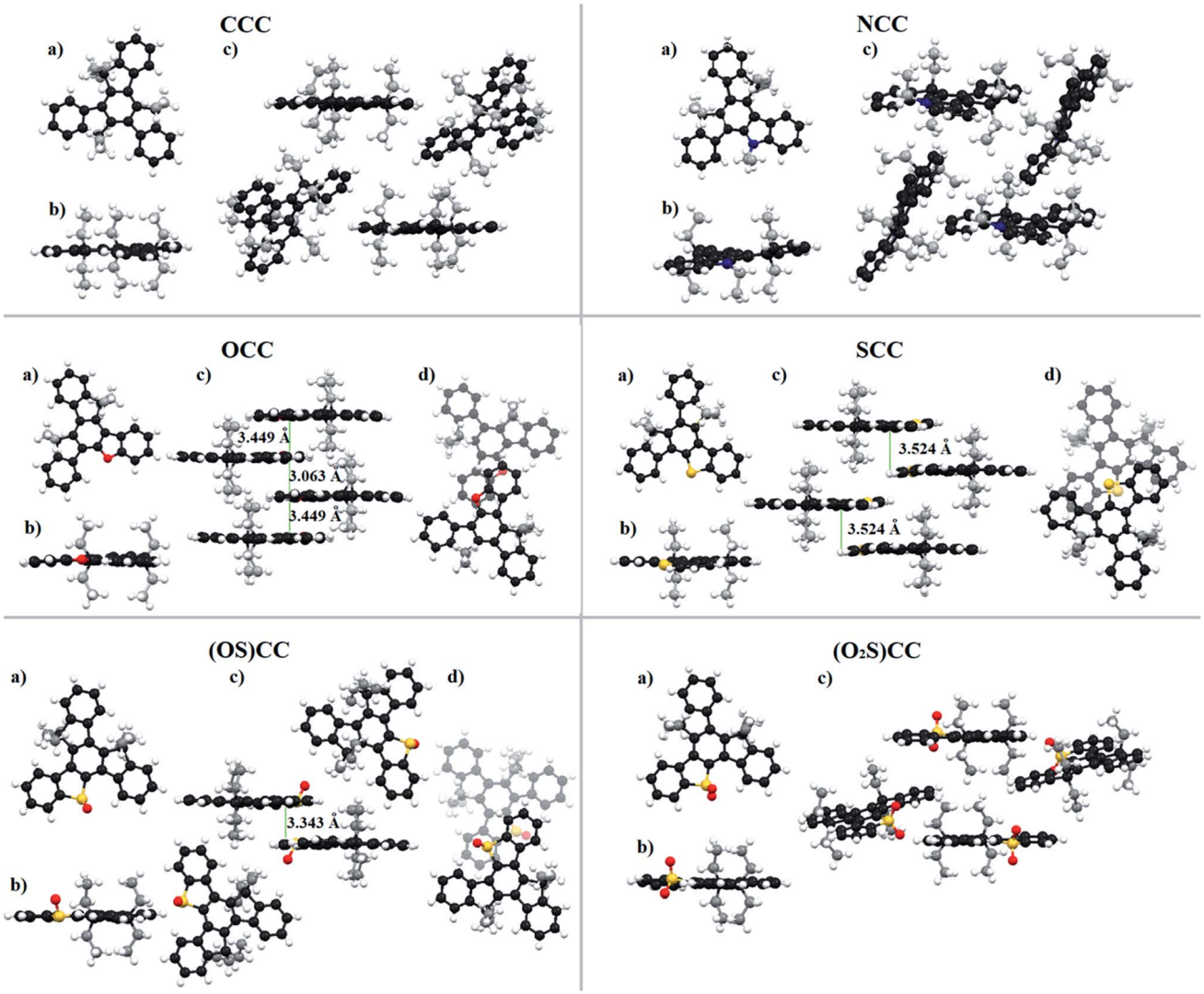

Fig. 6 Crystal structure of 5-heterotruxenes: (a) single molecule – top view, (b) single molecule – side view, (c) molecule arrangement in the crystal, (d) dimer structure – top view. For the clarity, carbon atoms of alkyl chains are marked gray. Figure made on the basis of published CIF files.[57,58]

and Table 2). A common feature for **CCC** and its mono-heteroanalogues is an evident rise in the intensity of low energy absorption bands. This noticeable change suggests an increase in the permissive character of the first two electronic transitions, which may be caused by partial breaking of the molecular symmetry in the solid state. Crystallographic structure analysis of **CCC** indicates a slight deformation of the truxene core from its planarity, causing the lower symmetry of the molecule from C_{3h} to C_1. Fig. 6.[57] The presence of six ethyl groups in the **CCC** molecule, oriented above and below the plane of the aromatic system, effectively limits intermolecular interactions between the π-electron systems. For this reason, there are no shifts in the absorption bands when passing from a solution to a solid state. **NCC** molecule, under the influence of crystalline forces, undergoes more pronounced deformation from its planarity than **CCC**. This phenomenon also occurs in N-alkyl derivatives of 5,10,15-triazatruxene.[74] Abolition of the symmetry plane results in the change of orientation of the ethyl group attached to the nitrogen atom, which combined with the presence of the other four alkyl chains, effectively limits π-stacking. The consequence of this phenomenon, the same as for **CCC**, is the practical lack of a bathochromic shift between absorption spectra in the solution and the solid state.

The introduction of one oxygen or sulfur atom causes other changes in the crystallographic structure of 5-heterotruxenes than observed in **NCC**. The occurrence of the heteroatom, without alkyl substituent, enables π-stacking interactions, which is visible as red-shift of **OCC** and **SCC** absorption. **OCC** in the solid state forms dimers with an internal distance of 3.063 Å. The lack of an alkyl chain attached to the heteroatom enables effective aggregation, which is directly responsible for the 2024 cm^{-1} red-shift of the absorption spectrum in the solid. A bathochromic shift can also be observed in the case of **SCC**. A greater distance between molecules, 3.524 Å, results in a smaller red-shift value, 793 cm^{-1}. The observed changes between emission spectra in the solid of **SCC** and its mono oxidized form, **(OS)CC** indicates a strong interaction between the molecules of the last. In **(OS)CC** molecule, one side is shielded by oxygen attached to the sulfur, whereas the opposite side is prone to π-stacking interactions. Thus, the observed bathochromic shift is the result of interactions between the **(OS)CC** enantiomers in the dimeric system, with the intermolecular distance of about 3.343 Å. Sulfoxide **(OS)CC** and sulfone **(O_2S)CC** present no significant shifts between absorption bands in the solid and in the solution. Emission spectra in the solution and the solid for each of the compounds look quite different in shape. Such behavior is a result of reabsorption. Mutual distances of main bands are preserved, but the relative intensity has changed. The quantum emissions of **(OS)CC** and **(O_2S)CC** is reduced by passing from the solution to the solid state. As a result of the excitation of **(OS)CC**, excited dimers are created, which opens a new channel for nonradiative deactivation of the excited state. The experimental proof is a 3-fold increase of the nonradiative constant at unchanged radiative constant, compared to the constants obtained from the solution measurements. In the case of **(O_2S)CC**, the crystallographic structure reveals deformations within the SO_2 moiety, which may be directly responsible for a two-fold increase in the non-radiative constant and thus the decrease in the fluorescence quantum yield. Quantum yield efficiency in the solid state for presented truxenes varies from 0.3% to 22% for **(OS)CC** and **OCC**, respectively (Table 2). Molecules in a condensed phase face numerous limitations of degrees of freedom. Significantly hindered rotations and vibrations reduce the share of non-radiative processes lowering more than two times nonradiative constant. Moreover, slight deformation of planar **CCC** molecule increases the probability of two first electronic transitions. The synergy of both processes results in a more 2-fold increase of emission quantum yield in the solid. Surprisingly, despite the structural similarities between **CCC** and **NCC**, Fig. 6, for the latter 3-fold reduction of QY is observed. Replacement of $C(Et)_2$ moiety to N(Et) is accompanied by a change in hybridization from sp^3 to sp^2, leading to severe geometric consequences. Tetrahedral hybridization of the carbon atom in **CCC** forces the orientation of ethyl groups above and below the plane of the truxene, while trigonal hybridization of the nitrogen atom results in the arrangement of an alkyl chain along with the flat aromatic core of **NCC**. Hindering the rotation and vibration in the solid phase increases the interaction between the ethyl group with one of the three arms of the truxene system. It can be seen as twisting the entire π-electron system. The resulting stress within the **NCC** molecule opens a new channel of nonradiative relaxation, which is directly responsible for decreasing the quantum yield of fluorescence in the crystalline phase. The decrease of emissive properties observed for **OCC** and **SCC** in the solid suggests an additional non-radiative channel. A slight deformation of the π-electron system is observed in both 5-heterotruxenes, but incomparably smaller than those present in **NCC** crystal. Therefore it cannot be the primary mechanism of nonradiative relaxation. In the crystallographic structure of **OCC** and **SCC**, pairs of interacting molecules can be distinguished. Thus one of the proposed explanation of lower quantum yield is creating excited dimers. This fact suggests that after absorption of light, excited dimers are created, which are responsible for the dissipation of energy accumulated in the excited state. A comparison of radiative and nonradiative constants between the solution and the solid state suggest such behaviour.

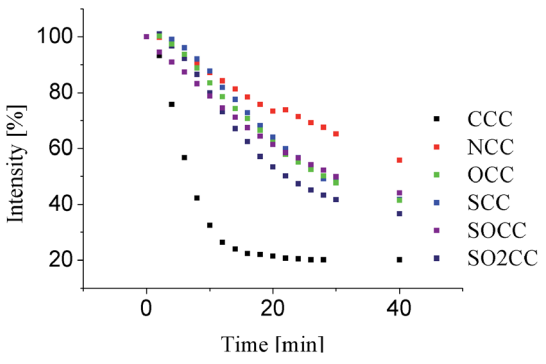

Fig. 7 Photochemical stability of **CCC** and 5-heterotruxenes in cyclohexane.

Table 3 Thermal properties of ethylated 5-heterotruxenes[a]

Compound	Heating I T_m [°C]	Cooling I T_c/T_g [°C]	Heating II $T_m/T_c/T_s$ [°C]	Cooling II T_c/T_g [°C]
CCC	217	99/—	217/—/—	99/—
NCC	181	—/112	—/—/103	—/112
OCC	214	—/112	222/125/—	—/112
SCC	209	—/98	209/167/—	—/98
(OS)CC	196	—/98	—/—/108	—/98
(O_2S)CC	222	—/99	—/—/112	—/99

[a] T_m – melting point, T_c – crystallization temperature, T_g – glass transition temperature, T_s – softening point.

Nearly 2-times and 1.5-times increase of radiative constant, for **OCC** an **SCC** respectively, indicate a formation of new radiative state presumably directly related to dimeric structure. On the other hand, the rise of nonradiative constant (more than 4-times for **OCC** and nearly 2.5-times for **SCC**) suggest the presence of a new nonradiative channel, being a consequence of π-stacking intermolecular interactions.

Photochemical stability

In order to determine photochemical stability compounds dissolved in cyclohexane were exposed to UV radiation. The determinant of photodegradation was a decrease in absorption. Cyclohexane guarantee chemical inactivity, whereas UV radiation, below 300 nm is absorbed by every compound, Fig. 7. Irradiation using monochromatic light form Xe 450 W lamp do

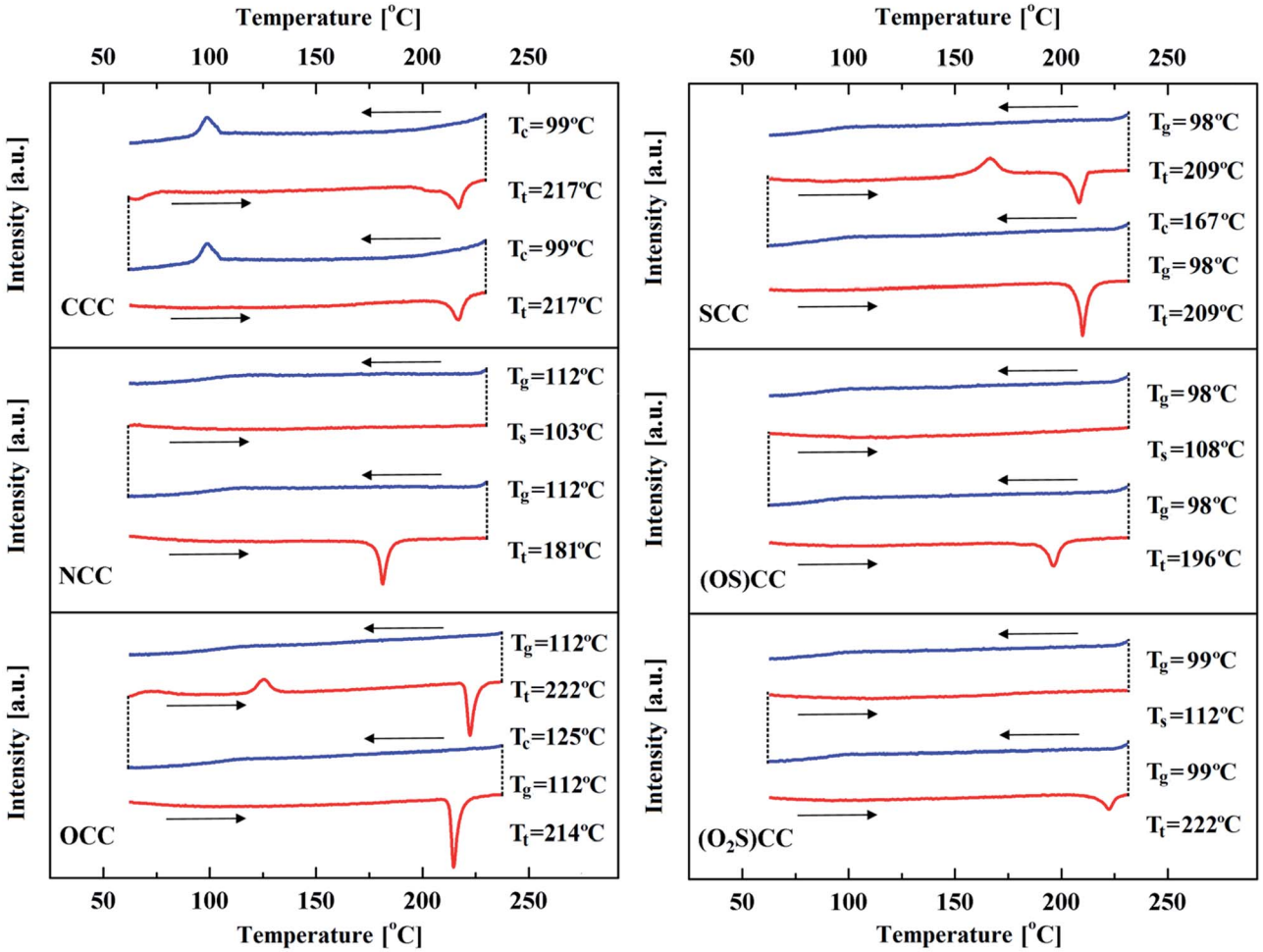

Fig. 8 DSC of ethylated 5-heterotruxenes, heating – red line, cooling – blue line. T_m –melting point, T_c –crystallization temperature, T_g – glass transition temperature, T_s –softening point.

not influence the absorption in hours' time, therefore 4 UV-C lamps, 55 W, were applied. Decrease in absorbance was clearly visible after second minute of irradiation. 2 minutes is an interval between consecutive cycles of irradiation and absorption measurement. On the Fig. 7 presented intensity is percentage decrease of absorbance. After 40 min all peaks vanishes and only broad band can be observed. Fig. 7 indicate that introduction of heteroatom into the truxene scaffold leads to greater photostability, in comparison to **CCC**. The best photochemical stability among 5-heterotruxenes is observed for **NCC** and the poorest for **(O$_2$S)CC**. The conducted measurements clearly indicates that introduction of one heteroatom significantly improves photochemical stability of every examined 5-heterotruxene.

Thermal properties

Structural changes in the solid, resulting from one heteroatom, affect not only the already discussed spectroscopic properties but also the thermal characteristics of 5-heterotruxenes (Table 3 and Fig. 8). Understanding the behaviour of those substances during heating or cooling is particularly important in the case of potential optoelectronic applications. Frequent melting and crystallization during the operation of the device can lead to premature degradation. In order to determine the thermochemical characteristics of 5-heterotruxenes, thermogravimetric analysis (TGA) and differential scanning calorimetry (DSC) were performed (Fig. 8). No weight loss of the sample was observed for each of truxenes **CCC**, **NCC**, **OCC**, **SCC**, **(OS)CC**, **(O$_2$S)CC** in the examined temperature range, 25–240 °C, which indicates their high thermal stability. As a result of heating, **CCC** melts at 217 °C. Subsequent cooling of **CCC** reveals a crystallization peak at 99 °C. Observed overcooling does not provide a stable glass formation. During the repetition of the heating and cooling cycles, no significant changes were observed, suggesting that both the starting sample and overcooled liquid crystalized in the same space group. Replacement of the diethyl methylene group in the ethyl substituted nitrogen atom, causes evident changes in thermal properties. **NCC** melts at 181 °C, which is far below the melting point of **CCC**, but, in contrast to its carbon analog, **NCC** forms stable glass with a glass transition temperature of 112 °C. Reheating of the sample results in softening at 103 °C. Subsequent heating and cooling of the examined **NCC** sample do not reveal any changes in the DSC diagram. Due to significant differences in the crystallographic structures of **OCC** and **SCC**, Fig. 6, different thermal behaviour of these substances can be expected. The **OCC** melting temperature is 214 °C, and the glass transition temperature is 112 °C, the same as in the case of **NCC**. Unlike the **NCC**, the recrystallization peak appears during reheating at 125 °C. Moreover, the newly formed crystalline phase melts at a slightly higher temperature of 222 °C, suggesting a different spatial structure than the starting sample. **SCC** behaves in a similar way to **OCC**. The **SCC** melts at 209 °C, and the observed glass transition temperature is 98 °C. As in the OCC case, it was reheating, which resulted in recrystallization at 167 °C. Again, subsequent heating and cooling of **SCC** sample do not reveal any changes in the DSC diagram.

The observed differences in melting and recrystallization temperatures of **OCC** and **SCC** are the result of differences in the structure of dimers observed in the crystalline phase. Distance between molecules in **OCC** dimer is 3.449 Å, and suggests stronger interactions as in the case of **SCC** dimer, 3.524 Å. Therefore, it is necessary to provide more energy to break the **OCC** dimeric systems than **SCC** one. As a result, the melting temperature for **OCC** is 5 °C higher than for **SCC**. On the other hand, stronger interaction between molecules in dimer allows faster reorientation of **OCC** molecules, which is visible in temperature of recrystallization, 42 °C lower than of **SCC**. Oxidized forms of **SCC** create stable glass. Melting temperature for **(OS)CC** is 14 °C lower whereas for **(O$_2$S)CC** is 13 °C higher compering **SCC**. Such differences can be explained by molecule arrangement and packing. Despite the lack of π-stacking, **(O$_2$S)CC** is such densely packed, that its melting temperature has the

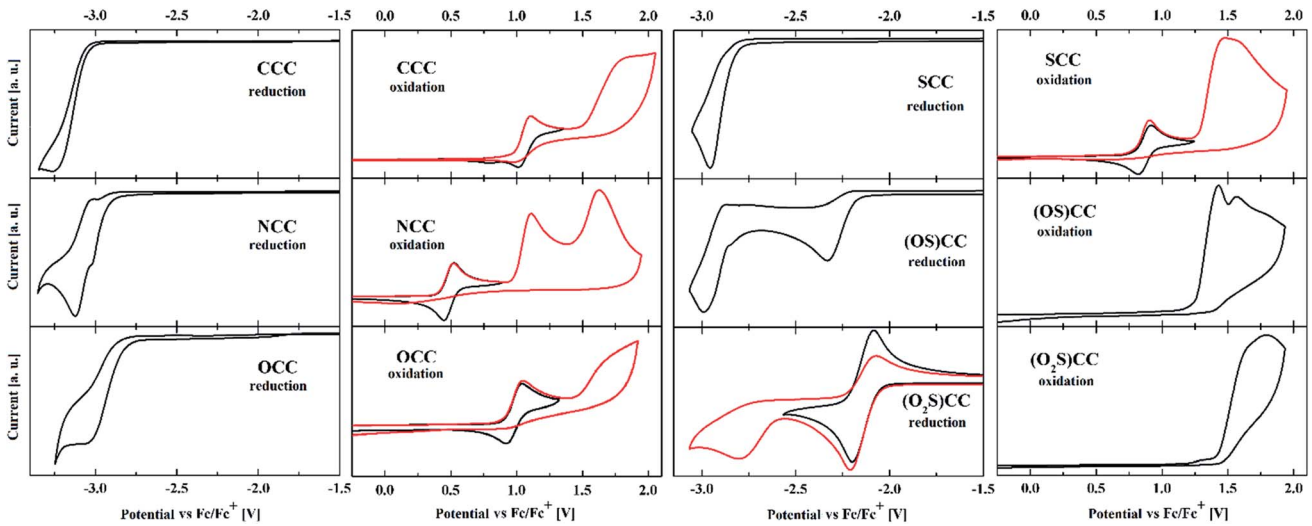

Fig. 9 Cyclic voltammograms of ethylated 5-heterotruxenes, reduction, and oxidation processes. Currents were normalized to allow better comparison of the data.

highest value. The glass transition temperatures are similar in both cases: 98 °C and 99 °C for **(OS)CC** and **(O_2S)CC**, respectively.

CCC crystalizes in the $Pna2_1$ space group. Regardless of the introduced heteroatom, **NCC**, **OCC**, and **SCC** crystallize in the same space group $P2_1/n$, despite apparent differences in packing. Only oxidized heterotruxenes **(OS)CC** and **(O_2S)CC** crystallize in other space groups *Pbca* and $P2_1/c$, respectively.

Electrochemical properties

The electrochemical character of obtained materials can also be modulated by the introduction of a specific heteroatom (Fig. 9 and Table 4). Different energies of HOMO and LUMO orbitals are reflected in accepting and donating properties of heterotruxenes. Voltammetric measurements were performed to investigate the redox properties of 5-heterotruxenes. In the positive potential range, **CCC**, **NCC**, **OCC**, and **SCC** undergo reversible oxidation with $E_{1/2}$ 1.06 V, 0.49 V, 0.97 V and 0.87 V *vs.* Fc/Fc^+, respectively, Table 4. Newly obtained **OCC** oxidation results differ from those obtained previously[57] by the absence of the irreversible oxidation process taking place at 0.76 V. Multiple studies for different **OCC** concentrations suggest that the oxidation process observed at 0.76 V may corresponds to the oxidation of **OCC** adsorbed onto glassy carbon electrode surface. Low solubility of **OCC** in acetonitrile, presence of electroactive material at electrode surface and the absence of oxidation at 0.76 V confirm this assumption at higher dilutions (2 mM). Further oxidation of the **OCC** leads to creation of instable products as the reduction of the reversible process is barely visible. However, potential reversal after the second oxidation peak, leads to important changes in the subsequent scans, suggesting adsorption of the product on the electrode. Electron withdrawing SO and SO_2 groups, present in sulfoxide **(OS)CC** and sulfone **(O_2S)CC** and respectively, cause significant stabilization of the HOMO orbital. Oxidation of those compounds leads to the creation of the reactive, positively charged ion and, as a result, to irreversible oxidation processes. On the other hand, electron attachment involves the significantly stabilized LUMO orbital. Among studied 5-heterotruxenes, this process is relatively high-energetic. Reduction leads to the formation of a highly reactive anion-radical. In the negative potential region, only **(O_2S)CC** reveals reversible reduction at −2.14 V *vs.* Fc/Fc^+. Interestingly, **(OS)CC** compound exhibits not one but two irreversible reductions at −2.31 and −2.97 V *vs.* Fc/Fc^+. Reversing potential scan after the first reduction process does not change the shape of the reduction peak, which indicate the irreversibility of the first reduction process of **(OS)CC**. (Fig. S7†). Insertion of electron withdrawing groups: SO and SO_2 is responsible for lowering of the LUMO, thus reduction processes of **(OS)CC** and **(O_2S)CC** undergo at more positive potentials. Reversible oxidation and irreversible reduction of **CCC**, **NCC**, **OCC** and **SCC** indicate them as donating subunits in new donor–acceptor systems. Analogously **(O_2S)CC** can act as a suitable electron acceptor. The packaging of 5-heterotruxenes in solids, combined with reversible oxidation processes, suggests their potential use as hole-transporting materials. The great advantage of those aromatic systems is the excellent solubility in most organic solvents, allowing the use of solution-processable methods for fabrication of optoelectronic devices. Nevertheless, it should be noted that in order to use the semiconductive properties of these substances, the π-electronic system of 5-heterotruxenes should have been previously modified, because the current energy of the HOMO level may be insufficient for most applications. Conducted spectroscopic characteristics supplemented with electrochemical measurements made it possible to prepare the experimental diagram of energy levels of 5-heterotruxenes (Fig. 10). The differences between experimental and calculated data result from the method used in calculations and solvation (vacuum in calculations and acetonitrile in the experiment). Despite the differences, the general trend concerning band gap value and the

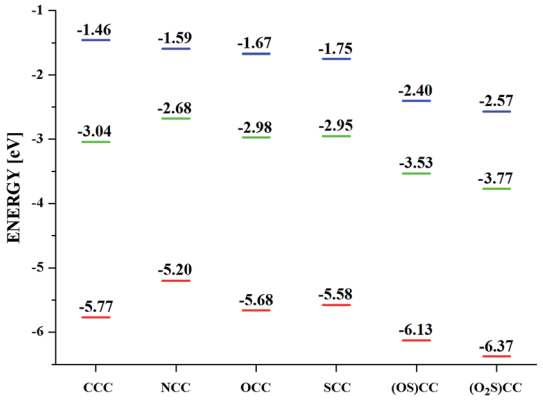

Fig. 10 Experimental energy diagram. HOMO level marked in red, LUMO in blue, and triplet state in green. HOMO and LUMO were derived from electrochemical oxidation and reduction, and the triplet state was estimated from the phosphorescence spectrum.

Table 4 Electrochemical data of ethylated 5-heterotruxenes in acetonitrile[a,b]

Compound	$E_{ox}{}^1$ [V]	$E_{ox}{}^2$ [V]	$E_{red}{}^1$ [V]	E_{HOMO} [eV]	E_{LUMO} [eV]	ΔE [eV]
CCC	1.06*	1.81	−3.25	−5.77	−1.46	4.31
NCC	0.49*	1.11	−3.12	−5.20	−1.59	3.61
OCC	0.97*	1.64	−3.04	−5.68	−1.67	4.01
SCC	0.87*	1.47	−2.96	−5.58	−1.75	3.83
(OS)CC	1.42	1.56	−2.31	−6.13	−2.40	3.73
(O_2S)CC	1.66	1.79	−2.14*	−6.37	−2.57	3.80

[a] E_{ox}/E_{red} – oxidation/reduction potential *vs.* Fc/Fc^+. * – reversible process ($E_{1/2}$). [b] $E_{HOMO} = -e(E_{ox}\,(V) + 4.71\,V)$, $E_{LUMO} = -e(E_{red}\,(V) + 4.71\,V)$.

relative location of the HOMO and the LUMO level are maintained. In addition, E_{0-0} (Table 1) obtained from the spectra is consistent with the electrochemical and theoretical data although the emission was measured in DCM. The presented diagram gives a quick insight into the actual electron structure of 5-heterotruxenes and determines their potential application. For example, for **NCC**, the energy of the HOMO level of −5.20 eV suggests its good hole conductivity. **OCC**, with T1 ← S0 transition, at a value of 2.70 eV, seems to be a promising candidate for a host material in a blue phosphorescent OLEDs.[75]

Experimental

General information

Studied compounds were synthesized according to literature procedures: **CCC**,[76] **OCC**,[57] **SCC**, **(OS)CC** and **(O_2S)CC**.[58] All data considering **CCC** and **OCC** was taken from the work of Górski *et al.*[57] A detailed protocol for obtaining **NCC** is available *via* the SI file. Optimization of the structures, energy levels calculation, and orbital visualization was realized by Gaussian 09 Rev. E.01 and Gauss View 5.0. Calculations were performed using DFT theory with the B3LYP/6-31g(d,p) functional and basis set for molecules in a vacuum. Absorption spectroscopy measurements were performed on UV-vis spectrophotometers UV-2401, for a solution and UV-2700, equipped with an integrating sphere, for a solid state, (Shimadzu, Japan). Emission spectra were obtained using the Fluorolog FL3-22 instrument equipped with an integrating sphere (Horiba Jobin Yvon, France). In fluorescence measurements, dichloromethane (freshly distilled) was were used as solutions and barium sulfate as dispersion matrix (spectroscopic grade, delivered by Shimadzu). In phosphorescence measurement carried out at 77 K methylcyclohexane (spectroscopic grade, Sigma-Aldrich) was used. XRD analysis was based on the already published article for **CCC**, **OCC**,[57] **NCC**, **SCC**, and **(OS)CC** and **(O_2S)CC**.[58] Photochemical stability measurement was realized using four UV-C lamps, (OSRAM UV-C lamp Puritec HNS L 2G11, 55 W). Each compound was dissolved in cyclohexane, and after exposure on UV-C irradiation, the decrease of one of the absorption peak was registered by the spectrophotometer UV-2700 (Shimadzu, Japan). The decrease of the absorption was measured at 305.5, 302.0, 301.5, 298.5, 288.5, and 287.0 nm for **CCC**, **OCC**, **NCC**, **SCC**, **(OS)CC** and **(O_2S)CC** respectively. Thermal analysis, including thermogravimetry and differential scanning calorimetry, were performed using the TGA-DSC 3+ STAR System (Mettler Toledo, Malaysia) under nitrogen flow. Cyclic voltammograms were collected using SP-300 potentiostat/galvanostat (Bio-Logic, France) driven by EC-Lab software v. 11. All electrochemical experiments were performed in a standard three-electrode setup. Tetra-*n*-butylammonium hexafluorophosphate ((TBA)PF_6, electrochemical grade), decamethylferrocene, and anhydrous acetonitrile (ACN), all obtained from Sigma-Aldrich, were used without further purification. Platinum spiral and silver wire were used as the counter and pseudo-reference electrodes, respectively. A glassy carbon working electrode of 2 mm in diameter was used throughout all the experiments. Decamethylferrocene was used as an internal potential reference, and all potentials were recalculated to its half-wave potential first and then referred to the ferrocene/ferrocenium redox couple for easier comparison with the literature data. The decamethylferrocene standard has been selected as it offers better stability of potential across large variety of solvents than ferrocene.[77] All voltammograms were recorded in 0.1 M (TBA) PF_6–ACN solutions deaerated before measurements by passing through a stream of argon N5.0.

Conclusions

The introduction of one heteroatom into the truxene core primarily disturbs the symmetry of the molecule and thus introduces an entirely new quality to the chemistry of these heptacyclic aromatic systems. For **NCC** and **OCC**, the fluorescence enhancement by symmetry breaking phenomenon (FESB) is observed, causing a 4-fold increase in the fluorescence quantum yield. The introduction of a sulfur atom allows the increase of spin–orbit coupling, which is especially important in the case of 3-generation OLED TADF emitters. Excellent thermal properties, characteristic for truxenes, are significantly improved in the case of 5-heterotruxenes. 5-Heterotruxenes present high thermal stability, up to 230 °C for **(OS)CC** and **(O_2S)CC**, and a clear tendency to form stable amorphous phases, especially **NCC**, **(OS)CC** and **(O_2S)CC**. Redox properties are undoubtedly related to the localization of electron levels. **NCC** has low reversible oxidation, at $E_{1/2} = 0.49$ V, thus presents the best electro donation properties, whereas **(O_2S)CC** has a reversible reduction at $E_{1/2} = -2.14$ V, pretending for suitable electron acceptor. Newly introduced synthesis of **NCC**, using precursor **1**, seems to be very promising for obtaining 5-heterotruxenes. It presents a simpler, more efficient, and universal path for obtaining 5-heterotruxenes, allowing the introduction of most atoms from the p-block. The donor or acceptor character of the molecule can be modulated by introducing the heteroatom into the truxene system. Such modulation enables the construction of a new donor–acceptor moiety for electronic (semiconductors or host materials in phosphorescent OLEDs), optoelectronic (emitting materials), or non-linear optics. Noteworthy is proposed, acid-promoted silicon-mediated cross-condensation, as the synthesis method of 7,12-dihydroindeno[1,2-*a*]fluorene derivatives, which opens new possibilities in designing 5-heterotruxenes, other nonsymmetrical truxenes, and related systems.

Conflicts of interest

There are no conflicts of interest to declare.

Acknowledgements

This work was supported by National Science Centre (grant no. FUGA 4, 2015/16/S/ST4/00427), and in part by the Institute of Physical Chemistry, Polish Academy of Sciences.

Notes and references

1 C. Destrade, P. Foucher, J. Malthete and T. H. Nguyen, On a Reentrant Isotropic Phase in Disc-like Liquid Crystals, *Phys. Lett.*, 1982, **88**(4), 187–190.
2 T. H. Nguyen, J. Malthete and C. Destrade, Reentrant Phenomenon in Disc-Like Liquid Crystal, *Mol. Cryst. Liq. Cryst.*, 1981, **64**, 291–298.
3 J. M. Buisine, R. Cayuela, C. Destrade and T. H. Nguyen, Dilatometric and Thermobarometric Measurements of Truxene Derivatives Exhibiting Inverted and Reentrant Sequences, *Mol. Cryst. Liq. Cryst.*, 1987, **144**(5), 137–160.
4 H. Yuasa, Y. Sato, Y. Kobori and M. Kobayashi, *Preparation of Liquid Crystal Compounds Having Photocurable Group*. JP 11092427 A, 1999.
5 F. Goubard and F. Dumur, Truxene: A Promising Scaffold for Future Materials, *RSC Adv.*, 2015, **5**, 3521–3551.
6 D. R. Vinayakumara, M. Kumar, P. Sreekanth, R. Philip and S. Kumar, Synthesis, Characterization and Nonlinear Optical Studies of Novel Blue-Light Emitting Room Temperature Truxene Discotic Liquid Crystals, *RSC Adv.*, 2015, **5**(34), 26596–26603.
7 L. Ma, Z. Wu, G. Zhou, F. Yuan, Y. Yu, C. Yao, S. Ning, X. Hou, Y. Li, S. Wang, *et al.*, The Molecular Picture of Amplified Spontaneous Emission of Star-Shaped Functionalized-Truxene Derivatives, *J. Mater. Chem. C*, 2015, **3**(27), 7004–7013.
8 W. Xu, J. Yi, W.-Y. Lai, L. Zhao, Q. Zhang, W. Hu, X.-W. Zhang, Y. Jiang, L. Liu and W. Huang, Pyrene-Capped Conjugated Amorphous Starbursts: Synthesis, Characterization, and Stable Lasing Properties in Ambient Atmosphere, *Adv. Funct. Mater.*, 2015, **25**(29), 4617–4625.
9 W. Lai, H. Zhang, T. Lu, X. Li and W. Huang, *Process for Preparation of Truxene-Based Organic Semiconductor Laser Material and Application*, CN 107445849 A, 2017.
10 M.-S. Yuan, Z.-Q. Liu and Q. Fang, Donor-and-Acceptor Substituted Truxenes as Multifunctional Fluorescent Probes, *J. Org. Chem.*, 2007, **72**(21), 7915–7922.
11 S. A. Wagay, I. A. Rather and R. Ali, Functionalized Truxene Scaffold: A Promising Advanced Organic Material for Digital Era, *ChemistrySelect*, 2019, **4**(42), 12272–12288.
12 M. A. Tehfe, J. Lalevée, S. Telitel, E. Contal, F. Dumur, D. Gigmes, D. Bertin, M. Nechab, B. Graff, F. Morlet-Savary, *et al.*, Polyaromatic Structures as Organo-Photoinitiator Catalysts for Efficient Visible Light Induced Dual Radical/Cationic Photopolymerization and Interpenetrated Polymer Networks Synthesis, *Macromolecules*, 2012, **45**(11), 4454–4460.
13 M.-A. Tehfe, F. Dumur, E. Contal, B. Graff, D. Gigmes, J.-P. Fouassier and J. Lalevée, Novel Highly Efficient Organophotocatalysts: Truxene–Acridine-1,8-Diones as Photoinitiators of Polymerization, *Macromol. Chem. Phys.*, 2013, **214**, 2189–2201.
14 J. Lalevée, M.-A. Tehfe, F. Dumur, D. Gigmes, B. Graff, F. Morlet-Savary and J.-P. Fouassier, Light-Harvesting Organic Photoinitiators of Polymerization. Pdf, *Macromol. Rapid Commun.*, 2013, **34**, 239–245.
15 K. Kailasam, M. B. Mesch, L. Möhlmann, M. Baar, S. Blechert, M. Schwarze, M. Schröder, R. Schomäcker, J. Senker and A. Thomas, Donor–Acceptor-Type Heptazine-Based Polymer Networks for Photocatalytic Hydrogen Evolution, *Energy Technol.*, 2016, **4**(6), 744–750.
16 Z. J. Wang, S. Ghasimi, K. Landfester and K. A. I. Zhang, Photocatalytic Suzuki Coupling Reaction Using Conjugated Microporous Polymer with Immobilized Palladium Nanoparticles under Visible Light, *Chem. Mater.*, 2015, **27**(6), 1921–1924.
17 T. H. Nguyen, R. Cayuela, C. Destrade and J. Malthete, Trithiatruxenes: A Family of Disc-like Mesogens with a New Polymorphism, *Mol. Cryst. Liq. Cryst.*, 1985, **122**, 141–149.
18 R. Cayuela, T. H. Nguyen, C. Destrade and A. M. Levelut, Two Families of Trithiatruxene Derivatives, *Mol. Cryst. Liq. Cryst.*, 1989, **177**, 81–91.
19 C. Destrade, T. H. Nguyen, L. Mamlok and J. Malthete, Trioxatruxenes: A New Family of Disc-Like Mesogens with a Complex Polymorphism, *Mol. Cryst. Liq. Cryst.*, 1984, **114**, 139–150.
20 G. H. Ahn, H. Du Kim, H. Il Lee, Y. B. Cha and S. R. Choi, *Organic Semiconductor Material Using Benzothiophene for Organic Thin Film Transistor*, KR 2011005476 A, 2011.
21 F.-W. Yen and C.-M. Teng, *Organic Optoelectronic Material and Use Thereof*, *US Pat.* 2016/0233427 A1, 2016.
22 Q. Xiao, T. Sakurai, T. Fukino, K. Akaike, Y. Honsho, A. Saeki, S. Seki, K. Kato, M. Takata and T. Aida, Propeller-Shaped Fused Oligothiophenes: A Remarkable Effect of the Topology of Sulfur Atoms on Columnar Stacking, *J. Am. Chem. Soc.*, 2013, **135**(49), 18268–18271.
23 A. Benito-Hernández, U. K. Pandey, E. Cavero, R. Termine, E. M. García-Frutos, J. L. Serrano, A. Golemme and B. Gómez-Lor, High Hole Mobility in Triindole-Based Columnar Phases: Removing the Bottleneck of Homogeneous Macroscopic Orientation, *Chem. Mater.*, 2013, **25**(2), 117–121.
24 F. Gallego-Gõmez, E. M. García-Frutos, J. M. Villalvilla, J. A. Quintana, E. Gutiérrez-Puebla, A. Monge, M. A. Díaz-García and B. Gómez-Lor, Very Large Photoconduction Enhancement upon Self-Assembly of a New Triindole Derivative in Solution-Processed Films, *Adv. Funct. Mater.*, 2011, **21**(4), 738–745.
25 E. Andrikaityte, J. Simokaitiene, A. Tomkeviciene, J. V. Grazulevicius and V. Jankauskas, Synthesis and Properties of Triindole-Based Monomers and Polymers, *Mol. Cryst. Liq. Cryst.*, 2014, **590**, 121–129.
26 G. Hu, S. P. Kitney, S. M. Kelly, W. Harrison, B. Lambert and M. O'Neill, Polymer Network Hole Transport Layers Based on Photochemically Cross-Linkable *N′N′*-Diallyl Amide Tri-N-Substituted Triazatruxene Monomers, *RSC Adv.*, 2018, **8**(16), 8580–8585.
27 H. Monobe, C. Chen, K.-Q. Zhao, P. Hu, Y. Miyake, A. Fujii, M. Ozaki and Y. Shimizu, Bipolar Carrier Transport in Tri-

Substituted Octyloxy-Truxene DLC, *Mol. Cryst. Liq. Cryst.*, 2011, **545**, 149–155.

28 X. Qian, Y.-Z. Zhu, J. Song, X.-P. Gao and J.-Y. Zheng, New Donor-π-Acceptor Type Triazatruxene Derivatives for Highly Efficient Dye-Sensitized Solar Cells, *Org. Lett.*, 2013, **15**(23), 6034–6037.

29 X. Qian, L. Lu, Y.-Z. Zhu, H.-H. Gao and J.-Y. Zheng, Triazatruxene-Based Organic Dyes Containing a Rhodanine-3-Acetic Acid Acceptor for Dye-Sensitized Solar Cells, *Dyes Pigm.*, 2015, **113**, 737–742.

30 B. Pan, Y.-Z. Zhu, D. Ye, F. Li, Y.-F. Guo and J.-Y. Zheng, Effects of Ethynyl Unit and Electron Acceptors on the Performance of Triazatruxene-Based Dye-Sensitized Solar Cells, *New J. Chem.*, 2018, **42**(6), 4133–4141.

31 P. Qin, P. Sanghyun, M. I. Dar, K. Rakstys, H. ElBatal, S. A. Al-Muhtaseb, C. Ludwig and M. K. Nazeeruddin, Weakly Conjugated Hybrid Zinc Porphyrin Sensitizers for Solid-State Dye-Sensitized Solar Cells, *Adv. Funct. Mater.*, 2016, **26**(30), 5550–5559.

32 T. Bura, N. Leclerc, S. Fall, P. Lévêque, T. Heiser and R. Ziessel, Absorption Tuning of Monosubstituted Triazatruxenes for Bulk Heterojunction Solar Cells, *Org. Lett.*, 2011, **13**(22), 6030–6033.

33 J.-L. Wang, J. Yan, Z.-M. Tang, Q. Xiao, Y. Ma and J. Pei, Gradient Shape-Persistent π -Conjugated Dendrimers for Light-Harvesting: Synthesis, Photophysical Properties, and Energy Funneling, *J. Am. Chem. Soc.*, 2008, **130**(30), 9952–9962.

34 J.-L. Wang, Z.-M. Tang, Q. Xiao, Y. Ma and J. Pei, Star-Shaped D-π-A Conjugated Molecules: Synthesis and Broad Absorption Bands, *Org. Lett.*, 2009, **11**(4), 863–866.

35 Y. Hao, M. Liang, Z. Wang, L. Wang, Y. Sun, Z. Sun and S. Xue, 3,4-Ethylenedioxythiophene as an Electron Donor to Construct Arylamine Sensitizers for Highly Efficient Iodine-Free Dye-Sensitized Solar Cells, *Phys. Chem. Chem. Phys.*, 2013, **15**(37), 15441–15449.

36 X. Zong, M. Liang, C. Fan, K. Tang, G. Li, Z. Sun and S. Xue, Design of Truxene-Based Organic Dyes for High-Efficiency Dye-Sensitized Solar Cells Employing Cobalt Redox Shuttle, *J. Phys. Chem. C*, 2012, **116**(20), 11241–11250.

37 C. Yao, Y. Yu, X. Yang, H. Zhang, Z. Huang, X. Xu, G. Zhou, L. Yue and Z. Wu, Effective Blocking of the Molecular Aggregation of Novel Truxene-Based Emitters with Spirobifluorene and Electron-Donating Moieties for Furnishing Highly Efficient Non-Doped Blue-Emitting OLEDs, *J. Mater. Chem. C*, 2015, **3**(22), 5783–5794.

38 S. C. Yuan, Q. Sun, T. Lei, B. Du, Y. F. Li and J. Pei, Star-Shaped Oligo(Fluorene Ethynylene)-Functionalized Truxene Derivatives: Synthesis, Characterization, and Their Size Effects, *Tetrahedron*, 2009, **65**, 4165–4172.

39 G.-L. Feng, W.-Y. Lai, S.-J. Ji and W. Huang, Synthesis of Novel Star-Shaped Carbazole-Functionalized Triazatruxenes, *Tetrahedron Lett.*, 2006, **47**(39), 7089–7092.

40 R. R. Reghu, D. Volyniuk, N. Kostiv, K. Norvaisa and J. V. Grazulevicius, Symmetry *versus* Asymmetry: Synthesis and Studies of Benzotriindole-Derived Carbazoles Displaying Different Electrochemical and Optical Properties, *Dyes Pigm.*, 2016, **125**, 159–168.

41 W.-Y. Lai, Q.-Y. He, D.-Y. Chen and W. Huang, Synthesis and Characterization of Starburst 9-Phenylcarbazole/Triazatruxene Hybrids, *Chem. Lett.*, 2008, **37**(9), 986–987.

42 J. Luo, B. Zhao, J. Shao, K. A. Lim, H. S. On Chan and C. Chi, Room-Temperature Discotic Liquid Crystals Based on Oligothiophenes—Attached and Fused Triazatruxenes, *J. Mater. Chem.*, 2009, **19**(44), 8327–8334.

43 W.-Y. Lai, R. Zhu, Q.-L. Fan, L.-T. Hou, Y. Cao and W. Huang, Monodisperse Six-Armed Triazatruxenes: Microwave-Enhanced Synthesis and Highly Efficient Pure Deep-Blue Electroluminescence, *Macromolecules*, 2006, **39**(11), 3707–3709.

44 P. Sam-ang, D. Raksasorn, M. Sukwattanasinitt and P. Rashatasakhon, A Nitroaromatic Fluorescence Sensor from a Novel Tripyrenyl Truxene, *RSC Adv.*, 2014, **4**(101), 58077–58082.

45 W. Huang, E. Smarsly, J. Han, M. Bender, K. Seehafer, I. Wacker, R. R. Schröder and U. H. F. Bunz, Truxene-Based Hyperbranched Conjugated Polymers: Fluorescent Micelles Detect Explosives in Water, *ACS Appl. Mater. Interfaces*, 2017, **9**(3), 3068–3074.

46 Y. Xu, X. Wu, Y. Chen, H. Hang, H. Tong and L. Wang, Star-Shaped Triazatruxene Derivatives for Rapid Fluorescence Fiber-Optic Detection of Nitroaromatic Explosive Vapors, *RSC Adv.*, 2016, **6**(38), 31915–31918.

47 N. Earmrattana, M. Sukwattanasinitt and P. Rashatasakhon, Water-Soluble Anionic Fluorophores from Truxene, *Dyes Pigm.*, 2012, **93**(1), 1428–1433.

48 Y. Xu, X. Wu, Y. Chen, H. Hang, H. Tong and L. Wang, Fiber-Optic Detection of Nitroaromatic Explosives with Solution-Processable Triazatruxene-Based Hyperbranched Conjugated Polymer Nanoparticles, *Polym. Chem.*, 2016, **7**(27), 4542–4548.

49 Y. Xu, H. Li, X. Wu, Y. Chen, H. Hang, H. Tong and L. Wang, Fluorescence Fiber-Optic Turn-on Detection of Trace Hydrazine Vapor with Dicyanovinyl-Functionalized Triazatruxene-Based Hyperbranched Conjugated Polymer Nanoparticles, *Polym. Chem.*, 2017, **8**(16), 2484–2489.

50 X.-C. Li, C.-Y. Wang, Y. Wan, W.-Y. Lai, L. Zhao, M.-F. Yin and W. Huang, A T-Shaped Triazatruxene Probe for the Naked-Eye Detection of HCl Gas with High Sensitivity and Selectivity, *Chem. Commun.*, 2016, **52**(13), 2748–2751.

51 K.-R. Wang, Y.-Q. Wang, H.-W. An, J.-C. Zhang and X.-L. Li, A Triazatruxene-Based Glycocluster as a Fluorescent Sensor for Concanavalin A, *Chem.–Eur. J.*, 2013, **19**(8), 2903–2909.

52 K.-R. Wang, H.-W. An, D. Han, F. Qian and X.-L. Li, Fluorescence Quenching of Triazatruxene-Based Glycocluster Induced by Peanut Agglutinin Lectin, *Chin. Chem. Lett.*, 2013, **24**(6), 467–470.

53 M. R. Maciejczyk, J. A. G. Williams, N. Robertson and M. Pietraszkiewicz, Monothiatruxene: A New Versatile Core for Functional Materials, *RSC Adv.*, 2017, **7**(78), 49532–49535.

54 M. R. Maciejczyk, S. Zhang, G. J. Hedley, N. Robertson, I. D. W. Samuel and M. Pietraszkiewicz, Monothiatruxene-

Based, Solution-Processed Green, Sky-Blue, and Deep-Blue Organic Light-Emitting Diodes with Efficiencies Beyond 5% Limit, *Adv. Funct. Mater.*, 2019, **29**(6), 1807572.

55 P. L. dos Santos, J. S. Ward, D. G. Congrave, A. S. Batsanov, J. Eng, J. E. Stacey, T. J. Penfold, A. P. Monkman and M. R. Bryce, Triazatruxene: A Rigid Central Donor Unit for a D–A3 Thermally Activated Delayed Fluorescence Material Exhibiting Sub-Microsecond Reverse Intersystem Crossing and Unity Quantum Yield *via* Multiple Singlet–Triplet State Pairs, *Adv. Sci.*, 2018, **5**(6), 1700989.

56 M.-S. Yuan, Q. Fang, Z.-Q. Liu, J.-P. Guo, H.-Y. Chen, W.-T. Yu, G. Xue and D.-S. Liu, Acceptor or Donor (Diaryl B or N) Substituted Octupolar Truxene: Synthesis , Structure and the Charge-Transfer Enhanced Fluorescence, *J. Org. Chem.*, 2006, **71**, 7858–7861.

57 K. Górski, J. Mech-Piskorz, K. Noworyta, B. Leśniewska and M. Pietraszkiewicz, Efficient Synthesis of 5-Oxatruxene and the Unusual Influence of Oxygen Heteroatom on Its Physico-Chemical Properties, *New J. Chem.*, 2018, **42**(8), 5844–5852.

58 K. Górski, J. Mech-Piskorz, B. Leśniewska, O. Pietraszkiewicz and M. Pietraszkiewicz, Synthesis and Reactivity of 5-Heterotruxenes Containing Sulfur or Nitrogen as the Heteroatom, *J. Org. Chem.*, 2019, **84**, 11553–11561.

59 S. Zhao, L. Kang, H. Ge, F. Yang, C. Wang, C. Li, Q. Wang and M. Zhao, Efficient One-Step Synthesis of C_3-Symmetrical Benzenoid Compounds Mediated by $SOCl_2$/EtOH, *Synth. Commun.*, 2012, **42**(24), 3569–3578.

60 B. P. Dash, R. Satapathy, E. R. Gaillard, J. A. Maguire and N. S. Hosmane, Synthesis and Properties of Carborane-Appended C_3-Symmetrical Extended π Systems, *J. Am. Chem. Soc.*, 2010, **132**(18), 6578–6587.

61 X. Zhang, Z. Wang, K. Xu, Y. Feng, W. Zhao, X. Xu, Y. Yan and W. Yi, HOTf-Catalyzed Sustainable One-Pot Synthesis of Benzene and Pyridine Derivatives under Solvent-Free Conditions, *Green Chem.*, 2016, **18**(8), 2313–2316.

62 Z.-H. Guo, C. Wang, Q. Zhang, S. Che, H.-C. Zhou and L. Fang, Cost-Effective Synthesis and Solution Processing of Porous Polymer Networks through Methanesulfonic Acid-Mediated Aldol Triple Condensation, *Mater. Chem. Front.*, 2018, **2**(2), 396–401.

63 C. W. Holzapfel and C. Dwyer, Stille and Suzuki Cross Coupling Reactions of *o*-Nitrophenyl Triflates: A Versatile Route to a Variety of Heterocycles, *Heterocycles*, 1998, **48**(8), 1513–1518.

64 A. W. Freeman, M. Urvoy and M. E. Criswell, Triphenylphosphine-Mediated Reductive Cyclization of 2-Nitrobiphenyls: A Practical and Convenient Synthesis of Carbazoles, *J. Org. Chem.*, 2005, **70**(13), 5014–5019.

65 K. Górski, J. Mech-Piskorz, B. Leśniewska, O. Pietraszkiewicz and M. Pietraszkiewicz, Toward Soluble 5,10-Diheterotruxenes: Synthesis and Reactivity of 5,10-Dioxatruxenes, 5,10-Dithiatruxenes, and 5,10-Diazatruxenes, *J. Org. Chem.*, 2020, **85**(7), 4672–4681.

66 S. Yamaguchi, Y. Itami and K. Tamao, Group 14 Metalloles with Thienyl Groups on 2,5-Positions: Effects of Group 14 Elements on Their π-Electronic Structures, *Organometallics*, 1998, **17**(22), 4910–4916.

67 C. Fave, M. Hissler, T. Kárpáti, J. Rault-Berthelot, V. Deborde, L. Toupet, L. Nyulászi and R. Réau, Connecting π-Chromophores by σ-P-P Bonds: New Type of Assemblies Exhibiting σ–π-Conjugation, *J. Am. Chem. Soc.*, 2004, **126**(19), 6058–6063.

68 A. M. Christianson, E. Rivard and F. P. Gabbaï, $1\lambda^5$-Stibaindoles as Lewis Acidic, Π-conjugated, Fluoride Anion Responsive Platforms, *Organometallics*, 2017, **36**, 2670–2676.

69 J. W. Levell, A. Ruseckas, J. B. Henry, Y. Wang, A. D. Stretton, A. R. Mount, T. H. Galow and I. D. W. Samuel, Fluorescence Enhancement by Symmetry Breaking in a Twisted Triphenylene Derivative, *J. Phys. Chem. A*, 2010, **114**(51), 13291–13295.

70 A. J. Tilley, R. D. Pensack, T. S. Lee, B. Djukic, G. D. Scholes and D. S. Seferos, Ultrafast Triplet Formation in Thionated Perylene Diimides, *J. Phys. Chem. C*, 2014, **118**(19), 9996–10004.

71 J. M. Andrés Castán, C. Dalinot, S. Dayneko, L. Abad Galan, P. Simón Marqués, O. Alévêque, M. Allain, O. Maury, L. Favereau, P. Blanchard, *et al.*, Synthesis, Characterization and Use of Benzothioxanthene Imide Based Dimers, *Chem. Commun.*, 2020, **56**(70), 10131–10134.

72 W. C. Martin, Table of Spin-Orbit Energies for p-Electrons in Neutral Atomic (Core) Np Configurations, *J. Res. Natl. Bur. Stand. – A. Phys. Chem.*, 1971, **75A**(2), 109–111.

73 H. Hiratsuka, Y. Tanizaki and T. Hoshi, Dichroism Analysis: The Allowed and Forbidden n–Π* Transition Bands of 1,3-Diazaazulene, *Spectrochim. Acta, Part A*, 1972, **28**(12), 2375–2386.

74 E. M. García-Frutos, E. Gutierrez-Puebla, M. A. Monge, R. Ramírez, P. de Andrés, A. de Andrés, R. Ramírez and B. Gómez-Lor, Crystal Structure and Charge-Transport Properties of N-Trimethyltriindole: Novel p-Type Organic Semiconductor Single Crystals, *Spectrochim. Acta, Part A*, 2009, **10**(4), 643–652.

75 Y. Tao, C. Yang and J. Qin, Organic Host Materials for Phosphorescent Organic Light-Emitting Diodes, *Chem. Soc. Rev.*, 2011, **40**(5), 2943–2970.

76 M.-S. Yuan, Q. Fang, Z.-Q. Liu, J.-P. Guo, H.-Y. Chen, W.-T. Yu, G. Xue and D.-S. Liu, Acceptor or Donor (Diaryl B or N)Substituted Octupolar Truxene: Synthesis, Structure, and Charge-Transfer-Enhanced Fluorescence, *J. Org. Chem.*, 2006, **71**(20), 7858–7861.

77 I. Noviandri, K. N. Brown, D. S. Fleming, P. T. Gulyas, P. A. Lay, A. F. Masters and L. Phillips, The Decamethylferrocenium/Decamethylferrocene Redox Couple: A Superior Redox Standard to the Ferrocenium/Ferrocene Redox Couple for Studying Solvent Effects on the Thermodynamics of Electron Transfer, *J. Phys. Chem. B*, 1999, **103**(32), 6713–6722.